Surface and bulk magnetic properties of pyrite NiS_2: Magnetization and neutron-scattering studies

Tineke Thio and J.W. Bennett
NEC Research Institute, 4 Independence Way, Princeton, New Jersey 08540

T.R. Thurston
Brookhaven National Laboratory, Upton, New York 11973
(Received 26 January 1995)

In pyrite-structure antiferromagnetic NiS_2, the magnetic susceptibility $\chi(T)$ shows downward curvature above the Néel transition ($T_{N1} = 39.2$ K), suggesting that magnetic correlations persist to $T = 400$ K. However, neutron-scattering measurements indicate that the bulk magnetic behavior above T_{N1} is conventional. We present evidence that the unusual temperature dependence of $\chi(T)$ arises from a surface contribution. At $T_{N2} = 29.75$ K a transition occurs to a weakly ferromagnetic state, accompanied by a small structural distortion. We show that this distortion is not tetragonal as suggested previously, but is most likely rhombohedral. Below T_{N2}, $\chi(T)$ is anisotropic; our data suggest that in this range $\chi(T)$ is dominated by next-nearest-neighbor exchange interactions.

I. INTRODUCTION

The discovery of superconductivity in the oxide superconductors has emphasized how little is currently understood about highly correlated electronic systems. This has motivated us to study NiS_2, which belongs to a large system of pyrite-type materials with a very rich phase diagram in magnetic and transport properties.[1,2] A Mott-Hubbard metal-insulator transition[3] occurs in $NiS_{2-x}Se_x$ for $x \approx 0.5$. NiS_2 (vaesite) is an insulating antiferromagnet (AF), in which long-range order sets in at a Néel temperature $T_{N1} \approx 40$ K. At $T_{N2} \approx 30$ K a first-order transition occurs to a weakly ferromagnetic (WF) state.[4] A small structural distortion[5] accompanies this magnetic transition.

The structure of NiS_2 is conducive to magnetic frustration. The Ni atoms are arranged on a fcc lattice, which can be thought of as a collection of triangular plaquettes of spins. Such a triangular arrangement, together with the AF nearest-neighbor interactions, gives rise to geometric magnetic frustration, as is observed in kagomé systems[6] and pyrochlores.[7] In NiS_2, well above the Néel temperature the magnetic susceptibility $\chi(T)$ has a highly unusual temperature dependence: Its curvature is negative, unlike the case for a conventional AF obeying the Curie-Weiss law. It seems plausible that this unusual behavior arises from magnetic frustration, but this is in fact not the case. In this paper we show that many of the unusual magnetic properties of undoped NiS_2 arise from a surface contribution. This fact has important consequences in the interpretion of magnetic measurements on selenium-doped materials in the metal-insulator series.

We present magnetization and neutron-scattering studies on large single crystals of pure NiS_2. Both sets of measurements evince magnetic transitions at $T_{N1} = 39.1$ K and $T_{N2} = 29.75$ K, consistent with previous work. Inelastic neutron-scattering measurements above T_{N1} show that the Néel transition is very similar to that of a conventional AF. This suggests that frustration is not the cause of the unusual magnetic behavior in the bulk at temperatures well above T_{N1}. On the other hand, geometry-dependent magnetization measurements indicate that the unusual magnetic susceptibility at $T > T_{N1}$ can be attributed to a surface contribution.

In the weakly ferromagnetic state, the staggered moment lies in the (x, y) plane, but the spins are canted in the z direction by a canting angle of $\approx 0.1°$. Below T_{N2} the magnetic susceptibility shows an anisotropy which is consistent with the idea that $\chi(T)$ is dominated by next-nearest-neighbor interactions. The structural distortion which occurs at T_{N2} is not tetragonal, as previously suggested, but is likely to be rhombohedral.

The format of this paper is as follows: In Sec. II we discuss the experimental details. The results of the magnetization studies, and those of the x-ray- and neutron-scattering experiments, are described in Secs. III and IV, respectively. Sec. V contains a discussion, and we conclude in Sec. VI.

II. EXPERIMENTAL DETAILS

Large single crystals of NiS_2 were grown by the chemical vapor transport method, with bromine as the transport agent.[8] The starting materials were 99.999% pure Ni powder and S powder obtained from Aesar Johnson Matthey. A charge of 10–15 g presynthesized NiS_2 powder was placed in a quartz ampoule (17 mm inner diameter × 200 mm length), together with a small amount of Br_2 (100 ml at 25 °C). The sealed ampoule was placed in a 2-in.-i.d. three-zone tube furnace with 8- or 10-in. zones. Growth occurred at av-

erage temperatures $T_{avg} = 700$–$800\,^{\circ}C$ and in a temperature gradient $\nabla T = 0.8\,^{\circ}C/cm$, with the charge at the high-temperature end. Growth times of 300 h yielded 4–5-mm single crystals, shaped like truncated octahedra with shiny (100) and (111) facets. A 1350-h run yielded single crystals of volume $v \sim 0.3$ cm^3. This crystal growth method is known to produce sulfur-deficient crystals.[9,10] From measurements of the specific gravity $\rho_m = 4.38 \pm 0.02$ g/cm^3 and the room-temperature lattice constant $a = 5.688(2)$ Å, we deduce[9] a crystal composition NiS_y with $y = 1.92 \pm 0.02$.

The magnetization measurements were done with a Quantum Design superconducting quantum interference device (SQUID) magnetometer, in a temperature range 5–400 K and magnetic fields up to 5.5 T. Geometry-dependent magnetization data were taken on flat thin samples cleaved from crystals along (100) directions, in order to avoid surface damage from cutting or polishing.

The neutron-scattering experiments were carried out at beam line H4M of the High Flux Beam Reactor at Brookhaven National Laboratory and at beam line BT-9 at the NBSR research reactor at the National Institute of Standards and Technology. A number of experimental configurations were used depending on the measurement performed.

High-resolution x-ray-scattering experiments were performed on a powder sample at beam line X-7A at the National Synchrotron Light Source. Silicon (220) crystals were used as monochromator and analyzer, and the x-ray energy was set at 8 keV. In the scattering experiments the sample was cooled using closed-cycle helium cryostats, which achieved a temperature stability of ~ 0.1 K over several hours.

III. MAGNETIZATION MEASUREMENTS

The magnetization of a NiS_2 single crystal is plotted in Fig. 1 as a function of applied field, at various temperatures as indicated in the figure. At high temperatures, $M(H)$ is linear in H. Just below $T \approx 30$ K, $M(H)$ shows a first-order jump at a critical field H_c, indicating the weakly ferromagnetic nature of the magnetic order at low temperatures. $H_c(T)$ is isotropic for the three directions of the applied field, (100), (110), and (111), and increased rapidly as T is decreased below T_{N2}. The temperature dependence of H_c is consistent with the results of Kikuchi:[11] $H_c(T) = C(T_{N2} - T)$, with $T_{N2} = 29.75 \pm 0.05$ K and $C = 500 \pm 200$ T/ K. Well below T_{N2}, the jump in $M(H)$ occurs at $H = 0$. At finite magnetic field, the magnetization can be fitted to a linear field dependence, $M(H) = M_0 + \chi H$.

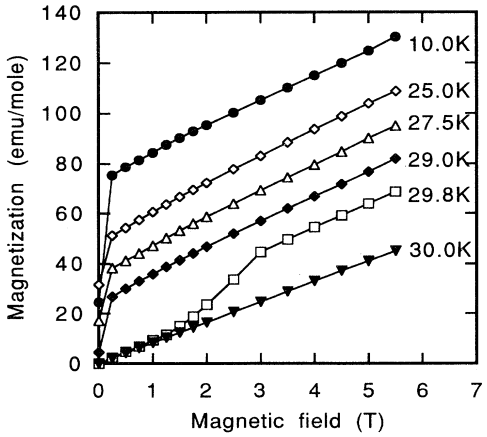

FIG. 1. Magnetization $M(H)$, at temperatures indicated. $H \parallel (111)$.

The temperature dependence of M_0 is plotted in Fig. 2. In a series of samples of which the masses varied by more than an order of magnitude, we find that M_0 scales with the sample mass; it is therefore a measure of the bulk WF moment. M_0 vanishes discontinously at $T_{N2} = 29.75 \pm 0.05$ K (see the inset of Fig. 2); below the transition it is anisotropic. We find $T = 0$ extrapolated values $M_0[100] = (2.3 \pm 0.1) \times 10^{-2} \mu_B$/Ni, $M_0[110] = (1.7 \pm 0.1) \times 10^{-2} \mu_B$/Ni, and $M_0[111] = (1.5 \pm 0.1) \times 10^{-2} \mu_B$/Ni.

Figure 3 shows $\chi(T)$ measured with the magnetic field applied in the (100), (110), and (111) directions. For all directions, $\chi(T)$ shows a first-order jump at $T = T_{N2}$, rising from $(8.0 \pm 0.1) \times 10^{-4}$ cm^3/mol (or $\chi = 2.9 \times 10^{-5}$ emu in dimensionless units) just above the transition to $(9.5 \pm 0.2) \times 10^{-4}$ cm^3/mol just below T_{N2}. $\chi[100]$ shows a sharp, ferromagneticlike maximum at the transition. On the other hand, $\chi[110]$ is only weakly temperature dependent below T_{N2}, whereas $\chi[111]$ decreases monotonically over the entire temperature range of the measurement. The $T = 0$ extrapolated values are $\chi[100] = (8.3 \pm 0.1) \times 10^{-4}$ cm^3/mol, $\chi[110] = (9.2 \pm 0.1) \times 10^{-4}$ cm^3/mol, and $\chi[111] = (1.05 \pm 0.05) \times 10^{-3}$ cm^3/mol, respectively.

Above $T_{N2} \approx 30$ K (see Fig. 2) the magnetization $M(H)$ is linear with the applied field up to $H = 5.5$ T and isotropic. The susceptibility $\chi(T) = dM/dH$ is shown by the open squares in Fig. 4. It shows a small cusp at a temperature which, in concert with the neutron-

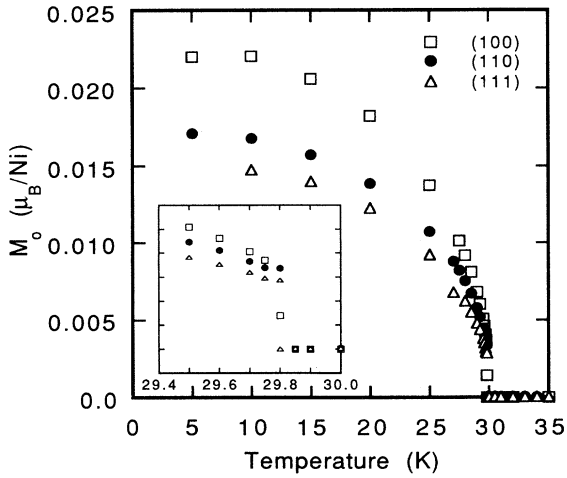

FIG. 2. Weak-ferromagnetic moment M_0 with $H \parallel (100)$ (open squares), $H \parallel (110)$ (solid circles), and $H \parallel (111)$ (triangles). Inset shows the data expanded around T_{N2}.

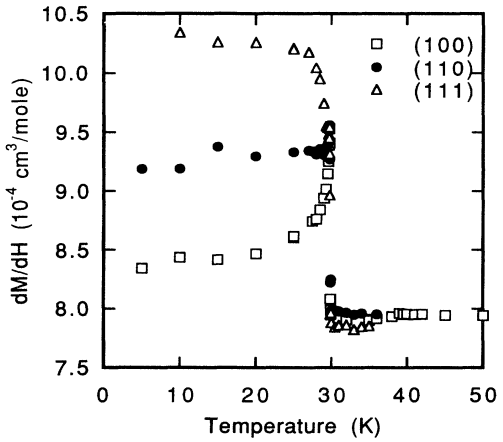

FIG. 3. Magnetic susceptibility $\chi(T) = dM/dH$ with H || (100) (open squares), H || (110) (solid circles), and H || (111) (triangles).

scattering measurements described below, we identify as the ordering temperature $T_{N1} = 39.1 \pm 0.1$ K (see inset). At high temperature, $\chi(T)$ has a highly unusual temperature dependence: Whereas in a conventional antiferromagnet the Curie-Weiss law causes $\chi(T)$ to have upward curvature, in NiS_2 the curvature in $\chi(T)$ is negative. This is the case for temperatures up to $T = 400$ K, or 10 times higher than T_{N1}.

We next investigate the possibility of a surface contribution to the magnetic properties. Most crystals are shaped like truncated octahedra and are cubelike in proportions. We have measured the magnetic susceptibility of a crystal which has been cleaved to a flat thin wafer (solid circles in Fig. 4), and which has a surface-to-volume ratio larger than that in the cubelike crystal by a factor ~10. The thin sample has a larger effective susceptibility than the cubelike sample at all temperatures. The magnetic susceptibilities measured were

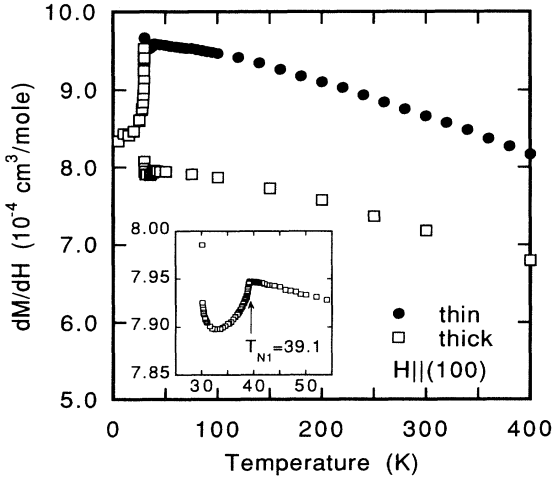

FIG. 4. Magnetic susceptibility $\chi(T)$, normalized to sample volume, for a cube-like sample (m = 210 mg, open squares) and a thin flat sample (solid circles).

of order ~ 10^{-3} cm^3/mol; for such small susceptibilities, the corrections for demagnetization due to sample geometry are less than ~ 0.04%.[12] But we note that to the $\chi(T)$ data plotted in Figs. 3 and 4 must be added the diamagnetic core contribution, which for NiS_2 is $\chi_{core} = -8.8 \times 10^{-5}$ cm^3/mol.[13]

A weak-ferromagnetic-like signal was observed between T_{N2} and T_{N1} at small magnetic fields, $H \approx 100$ G. Figure 5 shows the WF feature for two crystals, both cube like, one with mass $m = 52.1$ mg, the other with $m = 210$ mg. Above 40 K, the smaller sample has a larger magnetic moment than the large sample, when normalized to sample volume; this is consistent with the data in Fig. 4. Between 40 and 30 K, the WF signal has increased by 0.7% with respect to $\chi(T_{N1})$ in the larger sample, whereas in the smaller sample the change is 7%. A powder sample shows a WF signal about 15% of the susceptibility at T_{N1}. These results indicate that the sample surface makes a significant contribution to the WF signal.

IV. X-RAY- AND NEUTRON-SCATTERING EXPERIMENTS

Diffraction experiments were done to probe both the structural and magnetic properties of NiS_2. We begin this section with a description of a high-resolution x-ray-diffraction experiment which examined the structural distortion at T_{N2}. Figure 6 shows the full width at half maximum (FWHM) of the (200), (222), and (440) structural x-ray-diffraction peaks in a powder sample as a function of temperature. The figure shows that as the temperature is lowered below T_{N2}, the FWHM of the (200) peak is unchanged, while that of both the (440) and (222) peaks broadens. The broadening is indicative of the structural distortion, which causes these peaks to split into two or more peaks. However, the magnitude of the distortion is so small that the multiple peaks are not resolved by the spectrometer, and a refinement of the low-temperature structure is not possible.

The first set of neutron-scattering experiments were

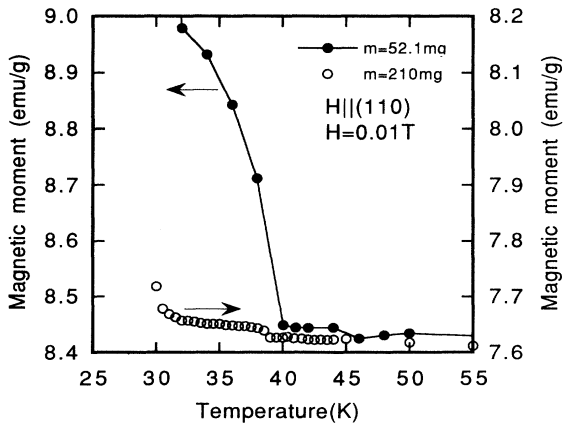

FIG. 5. Magnetization of a crystal with mass $m = 52.1$ mg (solid circles, left-hand scale) and $m = 210$ mg (open circles, right-hand scale), measured at $H = 0.01T$, H || (110).

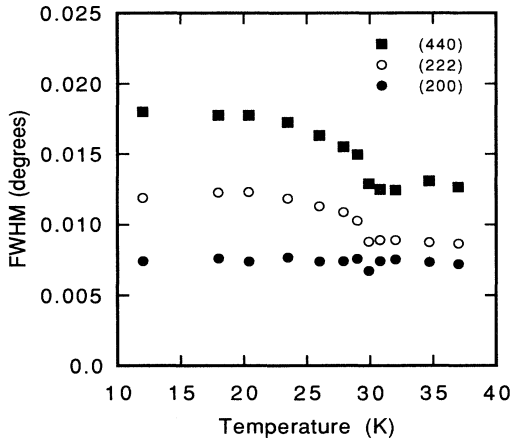

FIG. 6. Full widths of several x-ray-diffraction peaks in a powder sample: (200) (solid circles), (222) (open circles), and (440) (solid squares).

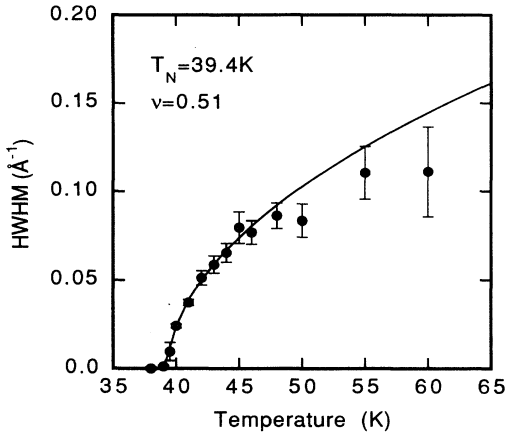

FIG. 7. Half-width of inelastic scattering peak at $\vec{q} = (1/2, 0, 0)$.

performed primarily to characterize the quality of our samples. A large single crystal ($v \sim 0.3$ cm^3) was mounted in an (h, l, l) zone, and neutron-scattering intensities at the (1/2, 0, 0) and (1/2, 1/2, 1/2) magnetic Bragg peaks were measured as a function of temperature in order to measure the magnetic order parameters. The results were very similar to those reported in Ref. 4 and are consistent with the magnetization data. At $T_{N2} = 30$ K the amplitude of the (1/2, 1/2, 1/2) peak jumps to zero. The (1/2, 0, 0) peak also shows a discontinuous change at T_{N2}, but to a finite value; at $T_{N1} = 40$ K it goes to zero continuously, indicating a second-order transition to the paramagnetic state. These results show that our crystals are of excellent quality and similar to the smaller crystals studied in the magnetization measurements and those studied previously.[4]

The second set of neutron-scattering experiments were devoted to measuring the critical scattering above T_{N1} around the (1/2,0,0) magnetic peak. The spectrometer was used in a two-axis mode (no analyzer crystal), and the three collimations between the source, the monochromator, the sample, and the detector were all 40′ full width at half maximum. Under these conditions the low-energy fluctuations are automatically integrated over, and the neutron-scattering intensity is approximately given by[14] $I(q,T) \sim k_B T \chi_{AF}(T)/(1 + q^2/\kappa^2)$, where $\chi_{AF}(T)$ is the susceptibility of the antiferromagnetic order parameter, $q = |q_1, q_2, q_3|$ is the deviation in $\vec{k}$ space from the (1/2,0,0) peak, and κ is the inverse correlation length of the antiferromagnetic fluctuations. We have measured the critical scattering along both the $(h,0,0)$ direction and the $(0,k,k)$ direction. The widths of the peaks in inverse angstroms for scans along these two directions were the same to within the errors. This is not surprising given the cubic structure of the material. In Fig. 7 we show the resolution-corrected half-width as a function of temperature for scans along the $(h,0,0)$ direction. The line in the figure represents a fit of the data to $\kappa(T) \sim (T/T_{N1} - 1)^{\nu}$, with $T_{N1} = 39.4 \pm 0.3$ K and $\nu = 0.51 \pm 0.05$. The antiferromagnetic susceptibility $\chi_{AF}(T)$ is shown in Fig. 8. The data have been fitted to the form $\chi_{AF}(T) \sim (T/T_{N1} - 1)^{-\gamma}$, yielding $T_{N1} = 39.3 \pm 0.2$ K and $\gamma = 0.9 \pm 0.1$. The Néel temperature found from these fits is consistent with that found from the magnetization measurements, $T_{N1} = 39.1 \pm 0.1$ K.

V. DISCUSSION

The magnetization and neutron-scattering data confirm previous studies of this compound:[4,11] Long-range AF order sets in at $T_{N1} = 39.2 \pm 0.1$ K and a transition occurs at $T_{N2} = 29.75 \pm 0.05$ K to a weakly ferromagnetic state. The neutron-scattering measurements of Miyadai *et al.*[4] suggest a type-I AF order $[\vec{q}_{AF} || (100)]$ between T_{N2} and T_{N1}, and a mixed type-I and type-II $[\vec{q}_{AF} || (111)]$ order in the WF state. For $T < T_{N2}$, the staggered moment lies in the (x, y) plane, but the spins are canted in the z direction.

The weak-ferromagnetic moment M_0 plotted in Fig.

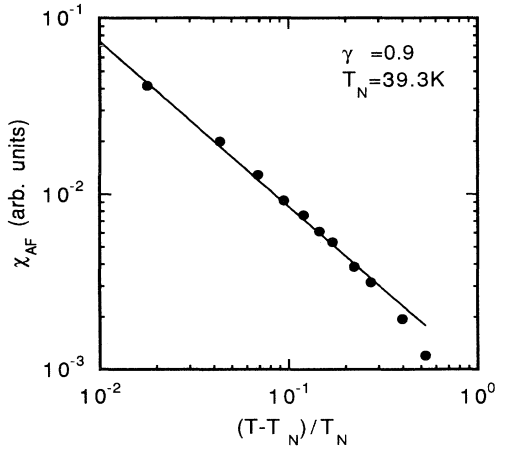

FIG. 8. Antiferromagnetic susceptibility measured at $\vec{q} = (1/2, 0, 0)$.

1 scales with sample volume and is therefore a measure of the bulk WF moment. The zero-temperature extrapolated values are slightly larger than those reported in previous work,[11] but they are approximately related by $M_0[100]$: $M_0[110] : M_0[111] = 1 : 1/\sqrt{2} : 1/\sqrt{3}$, consistent with the weak-ferromagnetic moment pointing in the [100] direction. The canting of the Ni spins gives $M_0[100] = M^{\dagger}\sin\theta$ where $M^{\dagger}$ is the staggered moment, and θ is the canting angle. With the staggered moment $M^{\dagger} = 1.3\mu_B$,[4] we find $\theta = (1.8 \pm 0.2) \times 10^{-3}$, or about 0.1°.

The magnetic susceptibility $\chi = dM/dH$ is anisotropic below T_{N2}. The magnitude of the anisotropy is only ~25%; however, the temperature dependence is strikingly different in the three crystal directions: Whereas $\chi[100]$ shows a ferromagneticlike peak at T_{N2}, again consistent with spin canting in the (100) direction, $\chi[110]$ is only weakly temperature dependent below T_{N2}, while $\chi[111]$ increases with decreasing T. The ferromagneticlike peak in $\chi[100]$ suggests that the WF moment is coupled to the staggered moment. Since the critical field needed to induce the weak ferromagnetic moment near T_{N2} is isotropic, off-diagonal elements in the nearest-neighbor exchange matrix are not likely to be the cause for the weak ferromagnetism. Since $\chi(T = 0) > \chi(T = T_{N1})$ in all directions, it is highly likely that in the WF phase the magnetic susceptibility is not dominated by nearest-neighbor exchange, but rather by exchange between next-nearest neighbors and possibly involving four-spin interactions.[15] Such higher-order interactions are also consistent with the coupling of the WF moment to $M^{\dagger}$.

Early measurements of the thermal expansion coefficient[5] indicated that a small structural distortion accompanies the first-order magnetic transition at $T_{N2} =$ 30 K. In fact, such a distortion must occur, since the space group of the high-temperature structure ($Pa\bar{3}$) does not allow ferromagnetic ordering. Nagata *et al.*[5] suggested that the low-temperature structure is tetragonal. However, our x-ray-scattering experiments strongly suggest that this is not the case, since there is no evidence of splitting of the (200) peak in the powder diffraction data of Fig. 6. From the diffraction data we conjecture that the low-temperature structure is rhombohedral.

Above T_{N1}, the magnetic susceptibility $\chi(T)$ shows a downward curvature; this is also found to be the case for other $NiS_{2-x}Se_x$ compounds with $x < 0.4$.[16] One possible reason for this is that the Ni spins remain correlated at temperatures much higher than T_{N1}, as is for instance the case in frustrated antiferromagnets. Geometric frustration is likely to occur in a fcc antiferromagnet, in which the spins are arranged on triangular plaquettes. Indeed, in isostructural pyrite-type MnS_2, which is also a fcc antiferromagnet, neutron-scattering measurements[17] show an incommensurate peak above the Néel transition at $T_N \approx 48$ K. Although the correlation length is very short (~ 10 Å), the magnetic correlations persist to at least $T = 150$ K.

However, in NiS_2 the fluctuations do not persist to high temperatures. In fact, the data in Figs. 7 and 8 indicate that the magnetic fluctuations above T_{N1} are conventional in character. From the temperature dependence of the magnetic correlation length and the scattering intensity, we find the exponents $\nu = 0.51 \pm 0.05$ and $\gamma = 0.9 \pm 0.1$. Both exponents are within errors of the mean-field values $\nu_{MF} = 1/2$ and $\gamma_{MF} = 1$, consistent with the majority of the data points being outside the critical region. The neutron-scattering data therefore show no evidence of magnetic frustration above T_{N1}; this confirms the suggestion from the low-temperature magnetic susceptibility that the next-nearest-neighbor exchange constants are relatively large,[15] resulting in the reduction of the nearest-neighbor AF frustration. Alternatively, the high concentration of sulfur vacancies[9] may be responsible for alleviating the magnetic frustration.

Moreover, the neutron-scattering data suggest that no anomalous effects are expected in magnetization measurements such as those shown in Fig. 4. In particular, Curie-Weiss behavior should be observed at high temperatures. We can reconcile this contradiction between our two different measurements by noting that the surface-to-volume ratio of the large single crystals used in the neutron-scattering measurements is much smaller than that of the samples used in the magnetization studies. Thus surface-related magnetic behavior was not visible above the instrumental background. In fact, from the magnetization measurements of Fig. 4 it is clear that an important contribution to the magnetic signal comes from the sample surfaces, since the magnetic susceptibility does not scale with the sample volume: A flat thin sample has a larger effective susceptibility than a cubelike sample with a lower surface-to-volume ratio. Between T_{N2} and T_{N1}, the sample surface also contributes a ferromagneticlike moment visible at small fields (see Fig. 5). The ferromagneticlike contribution is not apparent in $\chi(T)$ measured at high fields, since the surface moment is small compared to the total moment measured at high fields (see Fig. 4): In that case, $\chi(T)$ shows a cusp at T_{N1}, as expected for a conventional antiferromagnet.

We conclude that the surface magnetism of NiS_2 is significantly different from the bulk magnetism, although the crystals were too small to determine the surface contribution to the magnetic susceptibility above T_{N1} in a quantitative way. This is consistent with transport measurements of NiS_2, which have shown that at low temperatures the electrical transport is dominated by a highly conducting surface layer.[18] Certainly, the surface has a high density of dangling bonds which reconstruct in a local symmetry different from that found in the bulk. Alternatively, even though the bulk is itself sulfur deficient, diffusion of sulfur may cause the surface to be even more nickel rich. Either scenario gives rise to transport and magnetic properties at the surface which are distinct from those found in the bulk.

VI. CONCLUSION

In summary, magnetization and neutron-scattering measurements on single crystals of pure NiS_2 evince a Néel transition at $T_{N1} = 39.2 \pm 0.1$ K and a transition to a weakly ferromagnetic state at $T_{N2} = 29.75 \pm 0.05$

K. Below T_{N2}, $\chi(T)$ is anisotropic in the direction of the applied field, and is consistent with the WF moment pointing in the (001) direction; the canting angle is $\theta = (1.8 \pm 0.2) \times 10^{-3}$ rad. In this temperature range, $\chi(T)$ is dominated by next-nearest-neighbor exchange interactions; the crystal symmetry is lowered from cubic to possibly rhombohedral.

This fcc antiferromagnet shows no evidence for geometric frustration; instead, quasi-elastic neutron scattering in the critical region shows mean-field-like critical behavior, indicating that the magnetic ordering is quite conventional. It is the surface magnetism which is responsible for the unusual temperature dependence of the magnetic susceptibility above T_{N1}. A small weak-ferromagnetic moment observed between the transitions at T_{N1} and T_{N2} is also tracked to a surface contribution. These findings, together with the fact that the electrical transport is also affected by the surface layer, have serious implications on the interpretations made of experiments in the $NiS_{2-x}Se_x$ series. Although some techniques, such as neutron scattering or Mössbauer spectroscopy, probe the bulk of the material, other experiments, such as measurements of the Seebeck coefficient or of the heat capacity, may be much more susceptible to distortions due to a surface contribution. In the light of these results, it is time to reassess the available data on the $NiS_{2-x}Se_x$ system, and to separate the surface contributions from the properties intrinsic to the bulk.

ACKNOWLEDGMENTS

We gratefully acknowledge the help of P.M. Gehring with the neutron-scattering experiments at NIST and his critical reading of the manuscript, and the help of J.A. Hriljac and D.E. Cox with the x-ray-scattering experiments at NSLS at Brookhaven. We further acknowledge useful discussions with J.M. Tranquada. Work performed at Brookhaven is supported by the U.S. Department of Energy under Contract No. DE-AC02-76-CH00016.

[1] S. Ogawa, J. Appl. Phys. **50**, 2308 (1979).
[2] J.A. Wilson, in *The Metallic and Non-metallic States of Matter*, edited by P.P. Edwards and C.N.R. Rao (Taylor & Francis, London, 1985).
[3] F. Gautier *et al.*, Phys. Lett. **53A**, 31 (1975).
[4] T. Miyadai *et al.*, J. Phys. Soc. Jpn. **38**, 115 (1975).
[5] H. Nagata, H. Ito, and T. Miyadai, J. Phys. Soc. Jpn. **41**, 2133 (1976).
[6] A.P. Ramirez, G.P. Espinosa, and A.S. Cooper, Phys. Rev. Lett. **64**, 2070 (1990).
[7] B.D. Gaulin *et al.*, Phys. Rev. Lett. **69**, 3244 (1992).
[8] R.J. Bouchard, J.L. Gillson, and H.S. Jarrett, Mater. Res. Bull. **8**, 489 (1973).
[9] G. Krill *et al.*, J. Phys. C **9**, 761 (1976).
[10] M. Birkholz *et al.*, Phys. Rev. B **43**, 11 926 (1991).
[11] K. Kikuchi, J. Phys. Soc. Jpn. **47**, 484 (1979).
[12] J. Osborn, Phys. Rev. **67**, 351 (1945).
[13] C.J. O'Connor, Prog. Inorg. Chem. **29**, 203 (1982).
[14] W. Marshall and R. D. Lowde, Rep. Prog. Phys. **31**, 705 (1968).
[15] A. Yoshimori and H. Fukuda, J. Phys. Soc. Jpn. Lett. **46**, 1663 (1979).
[16] S. Sudo and T. Miyadai, J. Phys. Soc. Jpn. **54**, 3934 (1985).
[17] T. Chattopadyay, Th. Brückel, and P. Burlett, Phys. Rev. B. **44**, 7394 (1991).
[18] T. Thio and J.W. Bennett, Phys. Rev. B **50**, 10 574 (1994).